Dynamic Structure of Bombolitin II Bound to Lipid Bilayers as Revealed by Solid-state NMR and Molecular-Dynamics Simulation

Shuichi Toraya,[†] Namsrai Javkhlantugs,[†] Daisuke Mishima,[†] Katsuyuki Nishimura,[‡] Kazuyoshi Ueda,[†] and Akira Naito[†]*

[†]Faculty of Engineering, Yokohama National University, Yokohama, Japan; and [‡]Institute for Molecular Science, Okazaki, Japan

ABSTRACT Bombolitin II (BLT2) is one of the hemolytic heptadecapeptides originally isolated from the venom of a bumblebee. Structure and orientation of BLT2 bound to 1,2-dipalmitoyl-*sn*-glycero-3-phosphocholine (DPPC) membranes were determined by solid-state ^{31}P and ^{13}C NMR spectroscopy. ^{31}P NMR spectra showed that BLT2-DPPC membranes were disrupted into small particles below the gel-to-liquid crystalline phase transition temperature (T_c) and fused to form a magnetically oriented vesicle system where the membrane surface is parallel to the magnetic fields above the T_c. ^{13}C NMR spectra of site-specifically ^{13}C-labeled BLT2 at the carbonyl carbons were observed and the chemical shift anisotropies were analyzed to determine the dynamic structure of BLT2 bound to the magnetically oriented vesicle system. It was revealed that the membrane-bound BLT2 adopted an α-helical structure, rotating around the membrane normal with the tilt angle of the helical axis at 33°. Interatomic distances obtained from rotational-echo double-resonance experiments further showed that BLT2 adopted a straight α-helical structure. Molecular dynamics simulation performed in the BLT2-DPPC membrane system showed that the BLT2 formed a straight α-helix and that the C-terminus was inserted into the membrane. The α-helical axis is tilted 30° to the membrane normal, which is almost the same as the value obtained from solid-state NMR. These results suggest that the membrane disruption induced by BLT2 is attributed to insertion of BLT2 into the lipid bilayers.

INTRODUCTION

Bombolitins are five structurally and functionally related heptadecapeptides originally isolated from the venom of the bumblebee, *Megabombus pennsylvanicus*, and they lyse erythrocytes, release histamine from rat peritoneal mast cells, and enhance the activity of phospholipase A_2 (1). Bombolitins are similar in function and primary structure, especially for bombolitins I–III (BLT1–BLT3), whose primary structures are shown in Fig. 1. The underlined residues show homology among the three peptides. On the other hand, it has been reported that they show different secondary structural dependence on solution conditions such as pH, ionic strength, and peptide concentration (2–4), whereas they adopt predominately α-helical structure in solutions including sodium dodecyl sulfate (SDS) micelles (2,3). For the N-terminal region of BLT3, in which Lys^2 and Asp^5 are the same as in bombolitin II (BLT2), an α-helix formation is stabilized by a salt bridge between Lys^2 and Asp^5 at neutral pH (5). For an understanding of the cell-lysis mechanism of bombolitin, it is important to know the membrane-bound structure, as well as the peptide-lipid interactions. ^{1}H NMR using SDS micelles and molecular dynamics simulations showed that BLT2 was located on the surface of the micelles with the helical axis parallel to the water/micelle interface (6). In these systems, no bilayer interface is present as in biomembranes.

In solid-state NMR studies on membrane-bound peptides, mechanically oriented bilayers fixed between glass plates are frequently used to reveal orientation of the peptides to the bilayers with two-dimensional polarization inversion spin-exchange at the magic angle spinning experiments (7,8). Using this technique, a characteristic circular pattern, called a polarity index slant angle (PISA) wheel, is seen when the α-helix is formed in the membrane, and the shape of the wheel is sensitive to the tilting angle of the α-helix with respect to the bilayer normal (9–11). On the other hand, we have recently determined orientation of the α-helical axes of a honeybee toxic peptide, melittin, bound to dispersed 1,2-dilauroyl-*sn*-glycero-3-phosphocholine (DLPC), 1,2-dimirystoyl-*sn*-glycero-3-phosphocholine (DMPC), and 1,2-dipalmitoyl-*sn*-glycero-3-phosphocholine (DPPC) bilayers (12,13). The ^{13}C anisotropic and isotropic chemical shifts of ^{13}C-labeled carbonyl carbons of melittin were analyzed. These results indicate that melittin molecules adopt an α-helix with the tilt angles of the N-terminal helix at −33° and −36° and those of the C-terminal helix at 21° and 25° for DLPC and DPPC vesicles, respectively. Note that the tilt angle of the helix in melittin in the excess hydrated lipid bilayers is significantly different from that in the mechanically aligned lipid bilayers (14), because the extent of hydration is different. Orientation of the N-terminal α-helical axis of an opioid peptide, dynorphin A(1–17) bound to DMPC bilayers (15), as well as the structure and dynamics of those in the membrane-bound states, has been studied by solid-state NMR. In these peptide-lecithin bilayer systems, the vesicles fuse to form giant elongated vesicles that spontaneously align with their membrane planes parallel to the direction of the applied static magnetic field above the gel-to-liquid-crystalline

Submitted May 23, 2010, and accepted for publication September 20, 2010.

*Correspondence: naito@ynu.ac.jp

Editor: Marc Baldus.

0006-3495/10/11/3282/8 $2.00

doi: 10.1016/j.bpj.2010.09.060

BLT 1 : I K I T T M L A K L G K V L A H V[17]- NH_2
BLT 2 : S K I T D I L A K L G K V L A H V[17]- NH_2
BLT 3 : I K I M D I L A K L G K V L A H V[17]- NH_2

FIGURE 1 Primary structure of bombolitins I–III (BLT 1–BLT 3). The underlined residues show homology among the three peptides.

phase transition temperatures (T_c). Formation of these magnetically oriented vesicle systems (MOVS) accounts for membrane-orientation energy from interactions between magnetization of the numerous ordered lipid molecules and the magnetic field being larger than the thermal energy of the systems (12,16), as bicelles can magnetically orient (17,18). Since the peptides are bound to the magnetically oriented vesicles, the peptides can also orient to the magnetic field. ^{13}C NMR studies coupled with MOVS therefore reveal the orientation of the membrane-bound peptides (19). Other membrane-active peptides have also inserted in the membrane with a tilt angle of 50° (20).

A molecular dynamics simulation of melittin in a hydrated DPPC bilayer was performed. The simulation results show that the N-terminus of the peptide was protonated and embedded into the membrane in a transbilayer orientation perpendicular to the membrane surface, adopting a significant 25° tilt relative to the membrane normal (21). These results agree well with the experimentally determined structure in the DPPC bilayers (13). The structural properties of the opioid peptide dynorphin A(1–17) were studied by molecular dynamics simulation in DMPC bilayers. The N-terminal helical segment of dynorphin A was initially inserted in the bilayer in a perpendicular orientation with respect to the membrane plane and after 1 ns simulation, the helix axis achieved a tilt of ~50° relative to the bilayer normal (22). This value is larger than the value of 21° determined by solid-state NMR experiments (15).

In this work, it is shown that BLT2-DPPC lipid bilayers form MOVS above the T_c. We therefore investigate the structure, orientation, and dynamics of BLT2 bound to lipid bilayers using solid-state ^{13}C NMR spectroscopy. We also performed molecular dynamics simulations to investigate the orientational behavior of BLT2 inserted into the DPPC membrane using the CHARMM29 program. In concluding, we discuss the molecular mechanism of membrane lysis activity of BLT2.

MATERIALS AND METHODS

Sample preparation

Syntheses of 9-fluorenylmethoxycarbonyl (1-^{13}C)-L-amino acids were carried out with N-(9-fluorenylmethoxycarbonyl) succinimide (Watanabe Chemical Industries, Hiroshima, Japan) and (1-^{13}C)-labeled amino acids and (^{15}N)-labeled amino acids(Cambridge Isotope Laboratories, Andover, MA), following the method reported by Paquet (23). Singly labeled (1-^{13}C)Ile^3-BLT2, (1-^{13}C)Ile^6-BLT2, (1-^{13}C)Leu^7-BLT2, (1-^{13}C)Ala^8-BLT2, and (1-^{13}C)Leu^{10}-BLT2, and doubly labeled (1-^{13}C)Ile^3,(^{15}N)Leu^7-BLT2, (1-^{13}C)Leu^7,(^{15}N)Gly^{11}-BLT2, and (1-^{13}C)Leu^{10},(^{15}N)Leu^{14}-BLT2 molecules were synthesized using a 431A peptide synthesizer (Applied Biosystems, Foster City, CA). The crude peptide yielded by a cleavage reaction of the peptide-resin was purified with a Waters reverse-phase high-performance liquid chromatography system. The purity of the peptide was >95% as estimated by the area of the chromatogram. Trifluoroacetic acid was removed by keeping the sample in vacuo for 1 day.

DPPC was purchased from Sigma (St. Louis, MO) and used without further purification. A total amount of 50 mg powder containing BLT2 and DPPC at a peptide/lipid molar ratio of 1:10 was dissolved in 9 ml of chloroform. The solvent was subsequently evaporated in vacuo to prepare a homogeneous film, after which the residual solvent was removed under a high vacuum condition. A freeze-and-thaw cycle was repeated 10 times after the film was swelled with 300 μl of Tris buffer (20 mM Tris, 100 mM NaCl, pH 7.5). Glass and zirconia tubes with an outer diameter of 5 mm were filled with the sample and sealed hermetically. These samples were used to determine the chemical-shift interactions by NMR measurements of the BLT2-lecithin bilayer systems in the highly hydrated state.

The hydrated membrane dispersion was allowed to stand in the liquid-crystalline state for 1 h. Subsequently, the sample was frozen rapidly so that membrane disruption was not induced by BLT2. This frozen sample was lyophilized to retain the structure of the peptide in the lipid bilayers. The lyophilized powder was placed into zirconia tube with an outer diameter of 5 mm and subsequently used for measuring the principal values of the ^{13}C chemical-shift tensors of the ^{13}C-labeled carbonyl carbons and the ^{13}C-^{15}N interatomic distances in the immobile state.

NMR measurements

^{31}P and ^{13}C NMR measurements were performed on a Chemagnetics CMX infinity-400 NMR spectrometer (Fort Collins, CO) operating at the ^{31}P and ^{13}C resonance frequencies of 161.15 and 100.11 MHz, respectively. In the ^{31}P and ^{13}C NMR experiments of the hydrated BLT2-DPPC membrane dispersions, the free induction decay (FID) signals were obtained after 90°-excitation pulses of width 5.0 and 5.5 μs in the presence of high-power proton decoupling pulses of amplitude 50 and 45 kHz with repetition times of 2 and 5 s, respectively. A relatively low power decoupling field was used, because dipolar interactions are averaged out for the peptides in the liquid-crystalline phase, and heating of the samples was largely reduced. Lorentzian line broadenings of 60, 100, and 30 Hz were applied to the FID to obtain ^{13}C NMR spectra under the static, slow magic-angle spinning (slow MAS; spinning frequency of 100 Hz) and MAS (spinning frequency of 2 kHz) conditions, respectively, before Fourier transformations. To determine the principal values of the ^{13}C chemical-shift tensors of the carbonyl carbons, ^{13}C NMR spectra of the lyophilized powder samples were measured at 20°C using cross-polarization and MAS (CP-MAS) with a contact time of 1 ms, recycling time of 4 s, and spinning frequencies of 2 kHz. The principal values were determined by comparing the sideband patterns obtained from the CP-MAS experiments with the simulated spectra using the principal values of the chemical-shift interaction in the immobile state. ^{31}P and ^{13}C chemical-shift values were externally referred to 0 ppm of 85% H_3PO_4 for the phosphorus and 176.03 ppm for the carboxyl carbon of glycine from the shift for tetramethylsilane (TMS), respectively.

^{15}N rotational-echo double-resonance (REDOR) spectra were measured using an *xy*-4 irradiation pulse to compensate for the errors of the flip-angle, off-resonance effect, and fluctuation of the radio-frequency field for ^{13}C nuclei (24). The lengths of π pulses for ^{13}C and ^{15}N nuclei were 12.3 and 13.5 μs, respectively, and the recycle time was 4 s. The proton decoupling amplitude was 65 kHz. The rotor frequency was controlled to 6000 ± 2 Hz. REDOR and full echo spectra were recorded at various NcTr values from 6 to 24 ms, where Nc and Tr are the number of rotor cycle and rotor period, respectively. The REDOR differences were evaluated as

$$\Delta S/S_0 = \left(S_{\text{full echo}} - S_{\text{REDOR}}\right)/S_{\text{full echo}}, \quad (1)$$

where S_{REDOR} and $S_{full\ echo}$ are the peak intensities of REDOR and the full-echo spectrum, respectively. These REDOR differences were plotted against the NcTr values to fit the theoretically obtained curves to determine the ^{13}C-^{15}N interatomic distances.

Computational method

Molecular dynamics simulation was performed with the CHARMM29 program to investigate the orientation behavior of BLT2 inserted in the DPPC membrane. BLT2 backbone is a right-handed α-helix conformation with four positively charged residues, such as N-terminal Ser, and three Lys, and one negatively charged residue, Asp. The model of initial conformation of DPPC phospholipid bilayers in water developed by Feller and Pastor was used in this study (25). As an initial structure of the BLT2 in DPPC bilayers, BLT2 was first inserted into the membrane perpendicular to the membrane surface with its N-terminus close to the surface side. This is because the N-terminus of BLT2 is more hydrophilic than the C-terminus owing to the presence of the hydrophilic residues Ser^1, Lys^2, and Asp^5. Three chloride ions were added as counterions to neutralize the positively charged BLT2, and four NaCl molecules were added in the water region corresponding to a salt concentration of 0.1 M NaCl. The final combined model included one BLT2 molecule, 70 lipid molecules, 2083 water molecules, 4 sodium ions, and 7 chloride ions, and the total number of atoms in the system is 15,639.

Molecular dynamics simulation of the system was calculated with NPT ensemble (where number of atoms, pressure, and temperature are constant) with a pressure of 1 atm and a temperature of 323 K controlled by a Nose-Hoover thermostat (26,27). Periodic boundary conditions were assigned to the system with a rectangular box of dimensions 47.6 Å × 47.6 Å × 68 Å. The electrostatic interaction was calculated using the Ewald summation method (28). Trajectories of 2-ns dynamics for the system were calculated every 1 fs throughout the simulation. All the molecular dynamics calculations of CHARMM were performed using the standard lab-level workstation with AMD Opteron 285 dual core CPU.

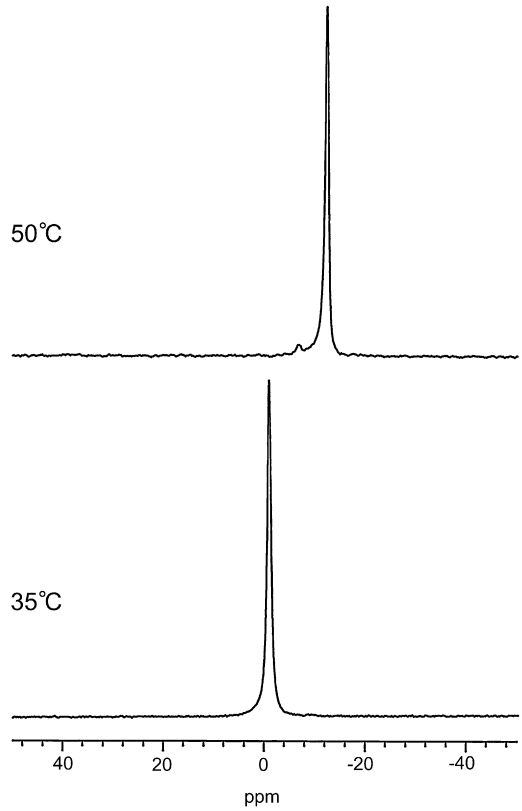

FIGURE 2 ^{31}P NMR spectra (1000 transients/spectrum) of BLT2-DPPC bilayer systems at 50°C ($>T_c$) and 35°C ($<T_c$) in the hydrated dispersion systems. The T_c of the DPPC bilayer is 41.5°C (29). The signals at 50°C and 35°C resonate at −12.2 and −0.8 ppm, respectively.

RESULTS AND DISCUSSION

Magnetic orientation of BLT2-DPPC vesicles

Fig. 2 shows temperature variations of ^{31}P NMR spectra of the BLT2-DPPC bilayer systems in the hydrated dispersion states. An isotropic signal resonated at −0.8 ppm was obtained at 35°C, which is a temperature below the T_c of pure DPPC (T_c = 41.5°C (29)). This indicates that the bilayer systems were disrupted to form small particles with a diameter of <100 nm (30) like micelles or discoidal micelles, as reported for melittin-lecithin bilayer systems (31), which have rapid random motions that show a narrow single line appearing at the isotropic chemical-shift value.

When the temperature is increased to 50°C, a temperature above the T_c, a signal appeared at −12.2 ppm, corresponding to the perpendicular component of the axially symmetric ^{31}P chemical-shift tensor. This observation clearly indicates that the disrupted small particles fuse to form large vesicles. It was therefore found that the membrane planes of the BLT2-DPPC vesicles magnetically orient parallel to the static magnetic field above the T_c to form elongated vesicles, MOVS, in the same manner as for melittin-lecithin bilayer systems (12,13).

^{13}C NMR spectra of carbonyl carbons of BLT2 bound to MOVS

Fig. 3 shows ^{13}C NMR spectra of (1-^{13}C)Ala^8 of BLT2 bound to DPPC bilayers at 50°C under static (Fig. 3 *a*), slow MAS (Fig. 3 *b*), and MAS (Fig. 3 *c*) conditions where MOVS are formed, as revealed by ^{31}P NMR experiments. Conformation-dependent ^{13}C isotropic chemical-shift values of various amino acid residues have been well correlated to the secondary structures in model peptides (32). Under the MAS condition (2-kHz spinning frequency (Fig. 3 *c*)), an isotropic signal appeared at 177.9 ppm and the chemical-shift value, δ_{iso}, revealed that the vicinity of Ala^8 adopts an α-helical structure. As a result of the slow-MAS (100-Hz spinning frequency) experiment performed to disturb the magnetic orientation, an axially symmetric powder pattern characterized by $\delta_\perp$ and $\delta_{//}$, was observed in the NMR spectrum (Fig. 3 *b*). This indicates that the helix of BLT2 rotates about a unique axis, which is equivalent to laterally diffusing in the membrane keeping the same tilt angle of the helical axis relative to the bilayer normal. Since narrow signals from free BLT2 molecules do not appear in the spectra, it is also apparent that all of the BLT2 molecules are bound to DPPC bilayers. Under the static condition

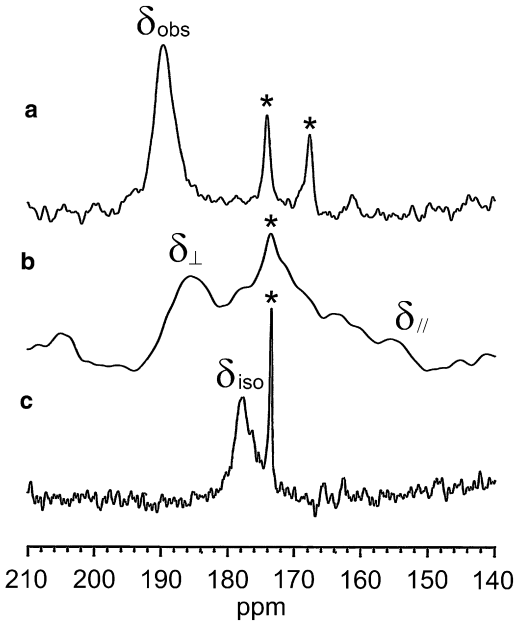

FIGURE 3 ^{13}C NMR spectra (2448–10,000 accumulated transients/spectrum) in the case of (1-^{13}C)Ala^{8}-BLT2 bound to hydrated DPPC bilayer systems at 50°C under the static (oriented) (*a*), slow MAS (spinning frequency of 100 Hz) (*b*), and MAS (spinning frequency of 2 kHz) (*c*) conditions. Signals denoted by asterisks are from the carbonyl carbons of the lipid.

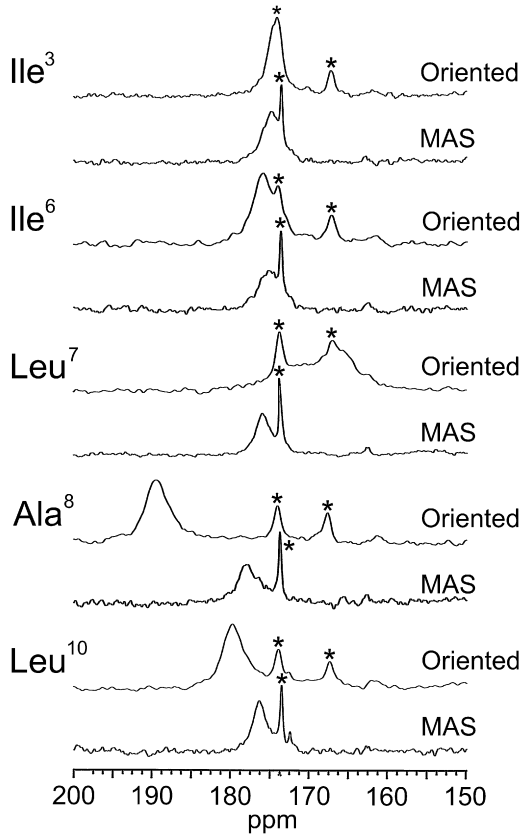

FIGURE 4 ^{13}C NMR spectra of carbonyl carbons of BLT2 bound to hydrated DPPC bilayers at 50°C under the static (oriented) and MAS conditions. A variety of carbonyl carbons were selectively labeled with ^{13}C nuclei. Symbols for the lipid signals are as defined in Fig. 3. There were 2448–5216 and 4704–11632 transients for the spectra under the static (oriented) and MAS conditions, respectively.

(Fig. 3 *a*), we observed a single signal resonating at 189.6 ppm. This chemical-shift value, δ_{obs}, is practically identical with that of the perpendicular component, $\delta_\perp$, of the axially symmetric powder pattern. Thus, the unique rotation axis of the helix is perpendicular to the membrane plane parallel to the magnetic field. We have shown that NMR signals of the carbonyl carbons in the helical peptides bound to magnetically oriented membranes depend on the tilt angle of the helical axis relative to the membrane normal and the location of the carbonyl carbon about the helical axis (13,15).

Fig. 4 shows ^{13}C NMR spectra of a variety of singly (1-^{13}C)-labeled BLT2 molecules bound to DPPC bilayers at 50°C. δ_{obs} and δ_{iso} values obtained under the static (oriented) and MAS conditions at Ile^{3}, Ile^{6}, Leu^{7}, Ala^{8}, and Leu^{10} were determined as summarized in Table 1. Using the correlation between isotropic ^{13}C chemical-shift values and secondary structure (25), it was revealed that BLT2 molecules bound to DPPC bilayers adopted an α-helical structure over the entire region (Table 1). Since δ_{obs} is identical with $\delta_\perp$, the ^{13}C chemical-shift anisotropy, $\Delta\delta = \delta_{//} - \delta_\perp$, of BLT2 bound to the oriented membranes can be calculated using the relation $\Delta\delta = 3(\delta_{iso} - \delta_{obs})$. Note that $\Delta\delta$ values change significantly, particularly between Leu^{7} and Ala^{8}. This indicates that the helix is rotated not about the helical axis but about the bilayer normal. Table 1 summarizes these anisotropies in the mobile state and the principal values of the ^{13}C chemical-shift tensors of BLT2 in the immobile state. As discussed later, these data are analyzed to determine the orientation of the helical axis of BLT2 bound to DPPC bilayers.

TABLE 1 ^{13}C chemical-shift values for BLT2 bound to DPPC bilayers

	δ_{iso} (ppm)*	Structure*	δ_{obs} (ppm)	$\Delta\delta$ (ppm)†	δ_{11} (ppm)‡	δ_{22} (ppm)‡	δ_{33} (ppm)‡
(1-^{13}C)Ile^{3}	174.9	α-helix	174.4	1.5	247.0	189.5	88.0
(1-^{13}C)Ile^{6}	175.3	α-helix	175.9	−1.8	244.5	192.5	89.0
(1-^{13}C)Leu^{7}	175.9	α-helix	165.8	30.3	244.5	192.5	89.0
(1-^{13}C)Ala^{8}	177.9	α-helix	189.6	−35.1	242.5	193.5	94.5
(1-^{13}C)Leu^{10}	176.5	α-helix	179.9	−10.2	244.5	192.5	89.0

NMR measurements of BLT2-DPPC bilayer systems were performed at 50°C.

*Typical ^{13}C chemical-shift values (δ_{iso} of α-helix, δ_{iso} of β-sheet) are (176.4, 171.8), (175.7, 170.5), and (174.9, 172.7) for (1-^{13}C)Ala, (1-^{13}C)Leu, and (1-^{13}C)Ile, respectively (32). Error ranges for δ_{iso} values were ±0.1 ppm.

†$\Delta\delta = 3(\delta_{iso} - \delta_{obs})$, where $\delta_{obs} = \delta_\perp$. Error ranges for $\Delta\delta$ and δ_{obs} values were ±0.6 and ±0.1, respectively.

‡δ_{11}, δ_{22}, and δ_{33} values were obtained from CP-MAS measurements of the lyophilized powder sample at 20°C. Error ranges of δ_{iso}, δ_{11}, δ_{22}, and δ_{33} values were ±0.1, ±1.0, ±1.0 and ±1.0 ppm, respectively.

^{15}N REDOR spectra of BLT2 bound to lyophilized lipid bilayers

Interatomic ^{13}C–^{15}N distances for (1-^{13}C)Ile^{3}–(^{15}N)Leu^{7}, (1-^{13}C)Leu^{7}–(^{15}N)Gly^{11}, and (1-^{13}C)Leu^{10}–(^{15}N)Leu^{14} were measured by means of a REDOR method (33) to determine the overall structure of BLT2 bound to lipid bilayers in the immobile state. Each full echo (Fig. 5, *upper traces*) and REDOR spectrum (Fig. 5, *lower traces*) of ^{15}N nuclei at the NcTr value of 18 ms are shown in the left column of Fig. 5. As revealed by plotting $\Delta S/S_0$ against NcTr values and fitting the calculated curve, the ^{13}C–^{15}N distances for (1-^{13}C)Ile^{3}–(^{15}N)Leu^{7}, (1-^{13}C)Leu^{7}–(^{15}N)Gly^{11}, and (1-^{13}C)Leu^{10}–(^{15}N)Leu^{14} were determined to be 4.4 ± 0.2, 4.3 ± 0.2, and 4.5 ± 0.2 Å, respectively (Fig. 5, *right column*). The error ranges were estimated by comparing the theoretical curves with the experimentally obtained values by looking at the fitting of four data points (only the best-fit curves are shown in Fig. 5). These distances are consistent with the case where these amino acid pairs may form hydrogen bonds to yield an α-helical structure. If the peptide adopts flexible α-helical structures, it causes longer ^{13}C–^{15}N distances, with their distributions for the structure in the immobile state. All of the distances for the BLT2 bound to the bilayers in the immobile state were in the range of a typical α-helical distance. These results suggest that the overall structure of BLT2 is a straight rod of α-helix in the liquid-crystalline membrane state without taking a kink structure.

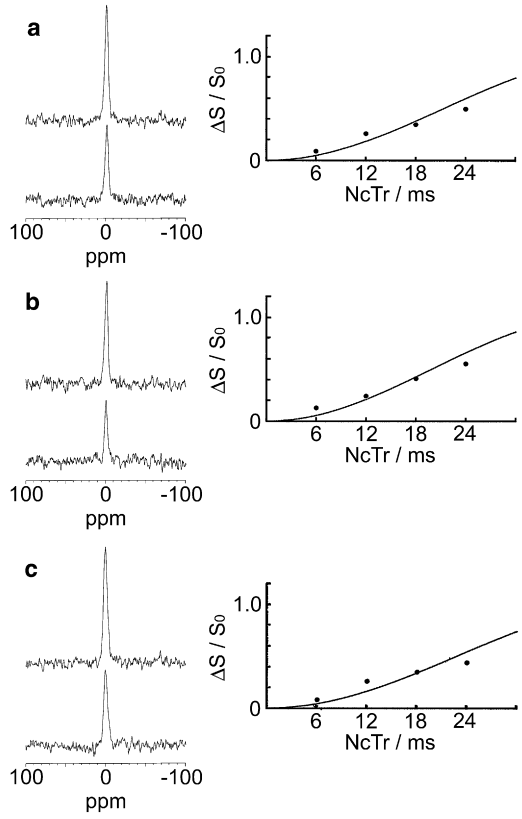

FIGURE 5 (*Left*) ^{15}N-REDOR (*lower traces*) and full echo (*upper traces*) spectra of doubly labeled molecules (1-^{13}C)Ile^{3},(^{15}N)Leu^{7}-BLT2 (*a*), (1-^{13}C)Leu^{7},(^{15}N)Gly^{11}-BLT2 (*b*), and (1-^{13}C)Leu^{10},(^{15}N)Leu^{14}-BLT2 (*c*) in lyophilized DPPC bilayer systems at an NcTr of 18 ms (10,000 transients). (*Right*) Plots of $\Delta S/S_0$ against NcTr values and best-fit curves corresponding to the spectra in *a-c*, showing ^{13}C–^{15}N interatomic distances of 4.4 ± 0.2, 4.3 ± 0.2, and 4.5 ± 0.2 Å, respectively.

Analysis of the dynamic structure of BLT2 bound to magnetically oriented vesicles

Rotational motion induced by lateral diffusion of the peptides anisotropically averages the chemical-shift tensors of the backbone carbonyl ^{13}C carbons, which show a large asymmetric powder pattern with anisotropy of ~150 ppm in the immobile states (Table 1). As described in our previous articles, a ^{13}C chemical-shift anisotropy (CSA) of a carbonyl carbon for the *i*th residue of an α-helical peptide rotating rapidly about an unique axis is expressed by

$$(\Delta\delta_{cal})_i = \frac{3}{2}\sin^2\zeta\left(\delta_{11}\cos^2\gamma_i + \delta_{33}\sin^2\gamma_i - \delta_{22}\right) + \left(\delta_{22} - \frac{\delta_{11} + \delta_{33}}{2}\right), \quad (2)$$

where ζ is the tilt angle of the helical axis to the unique axis, γ_i is the phase angle that defines the location of the carbonyl carbon of the *i*th residue in the helix, and (δ_{11}, δ_{22}, δ_{33}) are the principal values of ^{13}C CSA of the carbonyl carbon in the immobile state (13,15). Eq. 2 can be rewritten as

$$\overline{\Delta\delta_i} = (\Delta\delta_{cal})_i - \left(\delta_{22} - \frac{\delta_{11} + \delta_{33}}{2}\right). \quad (3)$$

In this equation, $\overline{\Delta\delta_i}$ values oscillate in the function of γ with the oscillation amplitude of (3/2)sin$^2\zeta$, which is referred to as the chemical-shift oscillation (13). Since the overall structure of BLT2 bound to the bilayers is a rigid α-helix, the orientation of the BLT2 molecules can be determined by calculating the root-mean-square deviations (RMSDs) of the experimental CSAs at Ile^{3}, Ile^{6}, Leu^{7}, Ala^{8}, and Leu^{10} from the theoretical CSAs using the equations

$$\mathrm{RMSD} = \sqrt{\sum_{i=1}^{5}\left\{(\Delta\delta_{obs})_i - (\Delta\delta_{cal})_i\right\}^2/5} \quad (4)$$

and

$$\gamma_{i+1} - \gamma_i = -100^\circ. \quad (5)$$

The latter equation shows that the difference in γ between contiguous residues is 100° because the peptide adopts a straight α-helical structure. A contour plot of the RMSDs against γ_{I6} (γ at Ile^{6}) and ζ is shown in Fig. 6. The least RMSD was clearly obtained at $\gamma_{I6} = 117^\circ$ and $\zeta = 33^\circ$.

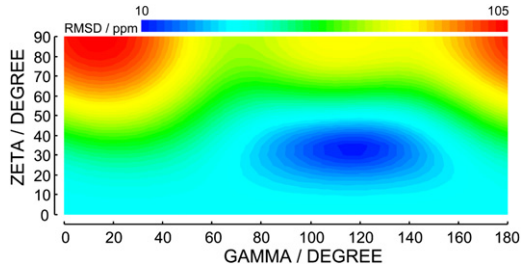

FIGURE 6 Contour plots of the RMSD between experimental and theoretical ^{13}C CSAs against the tilt angle of the helical axis of BLT2 relative to the membrane normal, ζ, and the phase angle of the carbonyl carbon of Ile^6 in the helix, γ_{I6}. RMSD values increase from blue to red. See online version for color.

For a straight α-helical structure, RMSD (γ_i, ζ) and RMSD (γ_i $-180°$, ζ) cannot be distinguished because of the symmetric property of Eq. 2. However, it was revealed that the α-helical BLT2 molecules laterally diffuse to rotate rapidly around the membrane normal with the tilt angle of the helix at 33° (Fig. 7 *a*). A comparison between the helical wheels with $\gamma_{I6} = 117°$ (Fig. 7 *b*) and $\gamma_{I6} = -63°$ (Fig. 7 *c*) shows that the bulky hydrophobic residues (Ile, Leu, and Val) are directed to the hydrophobic core of the bilayer when γ_{I6} is 117°. It is therefore reasonable that the orientation of BLT2 bound to the lipid bilayers is $\gamma_{I6} = 117°$ and $\zeta = 33°$. Further detailed structure of BLT2 bound to membrane is analyzed using the chemical-shift oscillation pattern for the ^{13}C CSAs of the carbonyl carbons (Eq. 3 and Fig. 8). The chemical-shift oscillation pattern clearly indicates that BLT2 takes a straight α-helix structure rather than the kink structure observed in melittin in the lipid bilayers (13). This straight α-helix structure is consistent with that determined by interatomic distances obtained from REDOR experiments, as also shown in Fig. 8 (*arrows*). The conformation of α-helix in the membrane would be stabilized by the salt bridge between the side chains of Lys^2 and Asp^5 at neutral pH (5). Since the side chains of Lys^9 and Lys^{12} are likely to interact electrostatically with negatively charged phosphate groups of the lipids, such interaction would tilt the peptide by 33° to the membrane normal under the helix motion (Fig. 7 *a*). The C-terminus is inserted into the hydrophobic core, but it does not completely penetrate the core, because the helix is not long enough to be transmembrane for the DPPC bilayer, whose thickness has been reported as 34.2 Å at 50°C (34).

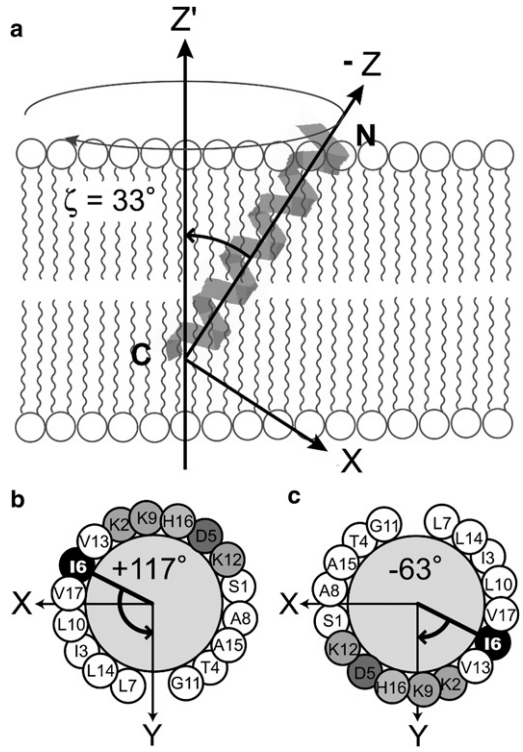

FIGURE 7 Schematic representations of the structure and orientation of BLT2 bound to the DPPC bilayer from analyses of the ^{13}C CSAs. (*a*) The *Z*′ axis is the rotation axis of BLT2, which is parallel to the membrane normal. The helix of BLT2 is tilted 33° relative to the membrane normal. (*b* and *c*) The possible helical wheels are $\gamma_{I6} = 117°$ (*b*) and $\gamma_{I6} = 63°$ (*c*).

Structure elucidation by molecular-dynamics simulation

A molecular-dynamics simulation was performed to investigate the orientation behavior of the BLT2 single molecule in the membrane system. The structure of the BLT2-DPPC bilayer system before the simulation is shown in Fig. 9 *a*. Although the initial orientation of the peptide was set parallel to the membrane normal, BLT2 began to tilt during the time course of the molecular dynamics simulation. Fig. 9 *b* shows the snapshot of the BLT2-DPPC bilayer system

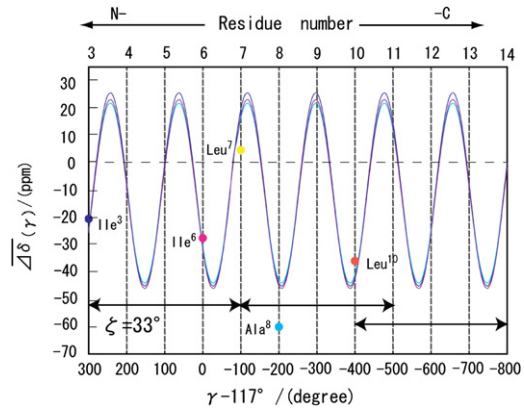

FIGURE 8 Chemical-shift oscillation patterns of BLT2. This chemical-shift oscillation pattern was obtained from the anisotropies of the carbonyl carbons of Ile^3 (*purple*), Ile^6 (*magenta*), Leu^7 (*yellow*), Ala^8 (*blue*), and Leu^{10} (*red*). ^{13}C–^{15}N interatomic distances for (1-^{13}C)Ile^3–(^{15}N)Leu^7, (1-^{13}C)Leu^7–(^{15}N)Gly^{11}, and (1-^{13}C)Leu^{10}–(^{15}N)Leu^{14} are 4.4 ± 0.2, 4.3 ± 0.2, and 4.5 ± 0.2 Å, respectively (*arrows*). See online version for color.

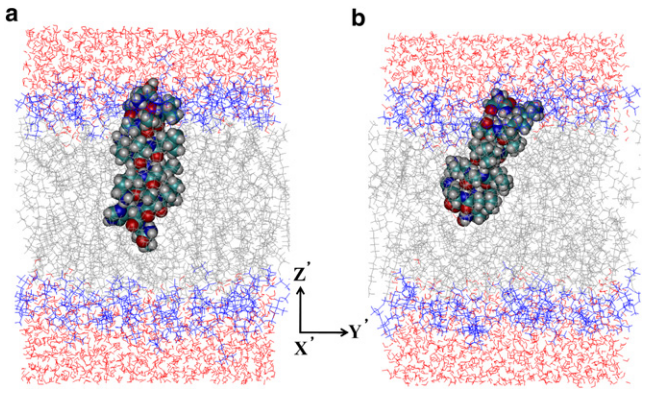

FIGURE 9 Snapshot of the BLT2/DPPC system before (*a*) and after (*b*) 2-ns simulation. The peptide backbone is shown in van der Waals format. Lipid headgroups, fatty acid chain groups, and water molecules are shown in blue, gray, and red, respectively. The C-terminus of BLT2 is inserted into the membrane, and sodium and chloride ions are not shown for simplicity. See online version for color.

after a 2-ns molecular-dynamics simulation. It is clear that the helical axis of BLT2 tilted after the 2-ns simulation. Fig. 10 shows the time course of the tilting angle during the 2-ns simulation. It can be seen that the BLT2 began to tilt until ~600 ps simulation time, when it oscillated and converged to an average value of 30° after 1 ns and kept that value until 2 ns. The tilted angle was calculated as the angle between the principal axis of the BLT2 molecule and the membrane normal. This averaged value is almost the same as the value obtained from the solid-sate NMR experiment. These results clearly show that the tilting behavior determined by the solid-state NMR experiments is reproduced by the molecular-dynamics simulation. A detailed analysis of the simulation will be discussed and published elsewhere shortly.

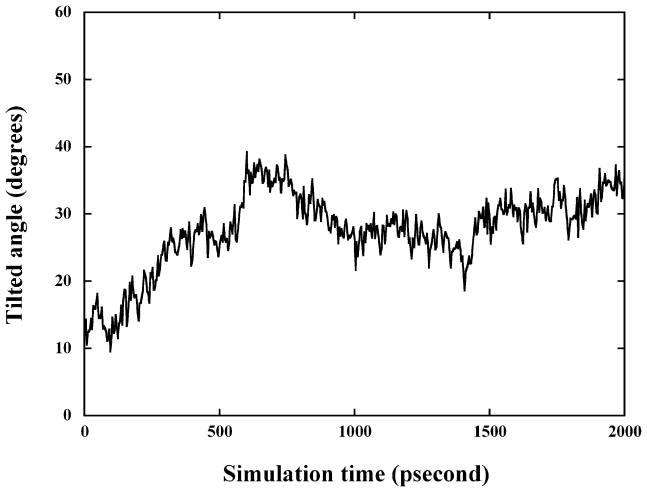

FIGURE 10 Tilted angle of BLT2 molecule as a function of simulation time. The tilted angle was calculated between the principal axis of the BLT2 molecule and the Z' axis, which is normal to the membrane.

Molecular mechanism of lysis and fusion in the BLT2-DPPC bilayer systems

The structure obtained from the solid-state NMR experiments and molecular-dynamics simulation suggests that the inserted helix perturbs the bilayer structure when BLT2 laterally diffuses in the membrane in a manner similar to that observed with melittin (13,35). The BLT2-induced perturbation promotes lipid mixing between adjacent vesicles to cause membrane fusion above the T_c. In the case of melittin, at a temperature close to the T_c, a large number of melittin molecules associate with each other by facing the hydrophilic side together and facing the hydrophobic side to the lipids to cause a large phase separation and partial disorder of lipids. When the temperature is below the T_c, bundles of melittin associate with each other. Consequently, small lipid bilayer particles are surrounded by the belt of melittin to be released from the vesicle. Subsequently, entire vesicles are dissolved into the buffer solution.

In the case of BLT2 in the lipid bilayers, a straight helix shows strong amphipathic behavior (Fig. 7 *b*); nevertheless, it is inserted into the lipid bilayer by tilting at an angle of 33° to the bilayer normal. It is therefore probable that helices may associate with each other along the hydrophilic face and act in a manner similar to that observed in the case of melittin.

CONCLUSIONS

It has been shown by solid-state ^{31}P NMR that below the T_c, BLT2 induces membrane disruption to form small particles and above the T_c it induces membrane fusion to form MOVS. Using the MOVS, we have determined the dynamic structure and orientation of BLT2 bound to DPPC lipid bilayers. The BLT2 molecule adopts a rigid straight α-helical structure whose helical axis rotates about the membrane normal at a tilt angle of 33° relative to the rotation axis. Molecular-dynamics simulation showed the same tilting behavior of BLT2 in the DPPC membrane as obtained using solid-state NMR. It is stressed that the C-terminus of BLT2 is inserted into the hydrophobic core with its bulky hydrophobic side facing the hydrophobic core. This structure indicates that the inserted α-helix perturbs the lipid-bilayer structure to weaken the interactions between lipid molecules. Consequently, the surface of the vesicles may fluctuate, and this can cause membrane fusion and disruption.

The authors thank the Research Center for Computational Science, Okazaki, Japan, for the use of a computer to perform part of the calculation.

This work was supported in part by Grants-in-Aid for Scientific Research on Priority Areas (19036006, 21017002) from the Ministry of Culture, Sports, Science and Technology of Japan.

REFERENCES

1. Argiolas, A., and J. J. Pisano. 1985. Bombolitins, a new class of mast cell degranulating peptides from the venom of the bumblebee *Megabombus pennsylvanicus*. *J. Biol. Chem.* 260:1437–1444.

2. Bairaktari, E., D. F. Mierke, …, E. Peggion. 1990. Conformational studies by circular dichroism, ^{1}H NMR, and computer simulations of bombolitins I and III in aqueous solution containing surfactant micelles. *Biochemistry.* 29:10090–10096.

3. Battistutta, R., A. Pastore, …, E. Peggion. 1995. Conformational properties of the amphipathic lytic polypeptide bombolitin II. A circular dichroism, NMR and computer simulation study. *Macromol. Chem. Phys.* 196:2827–2841.

4. Holtz, J. S. W., J. H. Holtz, …, S. A. Asher. 1999. Ultraviolet Raman examination of the environmental dependence of bombolitin I and bombolitin III secondary structure. *Biophys. J.* 76:3227–3234.

5. Ozdemir, A., I. K. Lednev, and S. A. Asher. 2002. Comparison between UV Raman and circular dichroism detection of short α helices in bombolitin III. *Biochemistry.* 41:1893–1896.

6. Monticelli, L., D. Pedini, …, E. Peggion. 2002. Interaction of bombolitin II with a membrane-mimetic environment: an NMR and molecular dynamics simulation approach. *Biophys. Chem.* 101-102:577–591.

7. Wu, C. H., A. Ramamoorthy, and S. J. Opella. 1994. High resolution heteronuclear dipolar solid-state NMR spectroscopy. *J. Magn. Reson.* A109:270–274.

8. Ramamoorthy, A., C. H. Wu, and S. J. Opella. 1999. Experimental aspects of multidimensional solid-state NMR correlation spectroscopy. *J. Magn. Reson.* 140:131–140.

9. Marassi, F. M., and S. J. Opella. 2000. A solid-state NMR index of helical membrane protein structure and topology. *J. Magn. Reson.* 144:150–155.

10. Marassi, F. M., C. Ma, …, S. J. Opella. 2000. Three-dimensional solid-state NMR spectroscopy is essential for resolution of resonances from in-plane residues in uniformly ^{15}N-labeled helical membrane proteins in oriented lipid bilayers. *J. Magn. Reson.* 144:156–161.

11. Wang, J., J. Denny, …, T. A. Cross. 2000. Imaging membrane protein helical wheels. *J. Magn. Reson.* 144:162–167.

12. Naito, A., T. Nagao, …, H. Saitô. 2000. Conformation and dynamics of melittin bound to magnetically oriented lipid bilayers by solid-state ^{31}P and ^{13}C NMR spectroscopy. *Biophys. J.* 78:2405–2417.

13. Toraya, S., K. Nishimura, and A. Naito. 2004. Dynamic structure of vesicle-bound melittin in a variety of lipid chain lengths by solid-state NMR. *Biophys. J.* 87:3323–3335.

14. Smith, R., F. Separovic, …, A. Makriyannis. 1994. Structure and orientation of the pore-forming peptide, melittin, in lipid bilayers. *J. Mol. Biol.* 241:456–466.

15. Uezono, T., S. Toraya, …, A. Naito. 2005. Structure and orientation of dynorphin bound to lipid bilayers by ^{13}C solid-state NMR. *J. Mol. Struct.* 749:13–19.

16. Naito, A., T. Nagao, …, H. Saitô. 2002. Dynorphin induced magnetic ordering in lipid bilayers as studied by ^{31}P NMR spectroscopy. *Biochim. Biophys. Acta.* 1558:34–44.

17. Sanders, II, C. R., and J. H. Prestegard. 1990. Magnetically orientable phospholipid bilayers containing small amounts of a bile salt analogue, CHAPSO. *Biophys. J.* 58:447–460.

18. Sanders, II, C. R., and J. P. Schwonek. 1992. Characterization of magnetically orientable bilayers in mixutures of dihexanoylphosphatidylcholine and dimyristoylphosphatidylcholine by solid-state NMR. *Biochemistry.* 31:8898–8905.

19. Naito, A. 2009. Structure elucidation of membrane-associated peptides and proteins in oriented bilayers by solid-state NMR spectroscopy. *Solid State Nucl. Magn. Reson.* 36:67–76.

20. Balla, M. S., J. H. Bowie, and F. Separovic. 2004. Solid-state NMR study of antimicrobial peptides from Australian frogs in phospholipid membranes. *Eur. Biophys. J.* 33:109–116.

21. Bachar, M., and O. M. Becker. 2000. Protein-induced membrane disorder: a molecular dynamics study of melittin in a dipalmitoylphosphatidylcholine bilayer. *Biophys. J.* 78:1359–1375.

22. Sankararamakrishnan, R., and H. Weinstein. 2000. Molecular dynamics simulations predict a tilted orientation for the helical region of dynorphin A(1–17) in dimyristoylphosphatidylcholine bilayers. *Biophys. J.* 79:2331–2344.

23. Paquet, A. 1981. Introduction of 9-fluorenylmethyloxycarbonyl, trichloroethoxycarbonyl, and benzyloxycarbonyl amine protecting groups into 0-unprotected hydroxyamino acids using succinimidyl carbonates. *Can. J. Chem.* 60:976–980.

24. Naito, A., and H. Saitô. 2002. Limit of accuracy of internuclear distances measured by REDOR. *Encycl. Nucl. Magn. Reson.* 9: 283–291.

25. Feller, S. E., R. M. Venable, and R. W. Pastor. 1997. Computer simulation of a DPPC phospholipid bilayer: Structural changes as a function of molecular surface area. *Langmuir.* 13:6555–6561.

26. Nose, S. 1984. A unified formulation of the constant temperature molecular dynamics methods. *J. Chem. Phys.* 81:511–519.

27. Hoover, W. G. 1985. Canonical dynamics: equilibrium phase-space distributions. *Phys. Rev. A.* 31:1695–1697.

28. Ewald, P. 1921. Die Berechnung optischer und elektrostatischer Gitterpotentiale. *Ann. Phys.* 369:253–287.

29. Van Dijck, P. W. M., B. De Kruijff, …, R. A. Demel. 1976. The preference of cholesterol for phosphatidylcholine in mixed phosphatidylcholine-phosphatidylethanolamine bilayers. *Biochim. Biophys. Acta.* 455:576–587.

30. Smith, I. C. P., and I. H. Ekiel. 1984. Phosphorus-31 NMR of phospholipids in membranes. *In* Phosphorus-31 NMR. Principles and Application. D. G. Gorenstein, editor. Academic Press, New York. 447–475.

31. Dufourcq, J., J.-F. Faucon, …, T. Gulik-Krzywicki. 1986. Morphological changes of phosphatidylcholine bilayers induced by melittin: vesicularization, fusion, discoidal particles. *Biochim. Biophys. Acta.* 859:33–48.

32. Saitô, H., and I. Ando. 1989. High-resolution solid-state NMR studies of synthetic and biological macromolecules. *Annu. Rep. NMR Spectrosc.* 21:209–290.

33. Gullion, T., and J. Schaefer. 1989. Rotational echo double-resonance NMR. *J. Magn. Reson.* 81:196–200.

34. Lis, L. J., M. McAlister, …, V. A. Parsegian. 1982. Interactions between neutral phospholipid bilayer membranes. *Biophys. J.* 37: 657–665.

35. Toraya, S., T. Nagao, …, A. Naito. 2005. Morphological behavior of lipid bilayers induced by melittin near the phase transition temperature. *Biophys. J.* 89:3214–3222.